



This is a repository copy of *TNT equivalency analysis of specific impulse distribution from close-in detonations*.

White Rose Research Online URL for this paper:  
<http://eprints.whiterose.ac.uk/168009/>

Version: Accepted Version

---

**Article:**

Grisaro, H.Y., Edri, I.E. and Rigby, S.E. [orcid.org/0000-0001-6844-3797](https://orcid.org/0000-0001-6844-3797) (2020) TNT equivalency analysis of specific impulse distribution from close-in detonations. *International Journal of Protective Structures*. ISSN 2041-4196

<https://doi.org/10.1177/2041419620972423>

---

Grisaro HY, Edri IE, Rigby SE. TNT equivalency analysis of specific impulse distribution from close-in detonations. *International Journal of Protective Structures*. November 2020. Copyright © 2020 The Author(s). DOI: 10.1177/2041419620972423. Article available under the terms of the CC-BY-NC-ND licence (<https://creativecommons.org/licenses/by-nc-nd/4.0/>).

**Reuse**

This article is distributed under the terms of the Creative Commons Attribution-NonCommercial-NoDerivs (CC BY-NC-ND) licence. This licence only allows you to download this work and share it with others as long as you credit the authors, but you can't change the article in any way or use it commercially. More information and the full terms of the licence here: <https://creativecommons.org/licenses/>

**Takedown**

If you consider content in White Rose Research Online to be in breach of UK law, please notify us by emailing [eprints@whiterose.ac.uk](mailto:eprints@whiterose.ac.uk) including the URL of the record and the reason for the withdrawal request.



[eprints@whiterose.ac.uk](mailto:eprints@whiterose.ac.uk)  
<https://eprints.whiterose.ac.uk/>

# TNT equivalency analysis of specific impulse distribution from close-in detonations

Hezi Y. Grisaro<sup>a,1</sup>, Idan E. Edri<sup>a</sup>, Samuel E. Rigby<sup>b</sup>

<sup>a</sup> Faculty of Civil & Environmental Engineering, National Building Research Institute, Technion - Israel Institute of Technology, Haifa, Israel

<sup>b</sup> Department of Civil & Structural Engineering, University of Sheffield, Mappin Street, Sheffield, S1 3JD, UK

## Abstract

Detonation of a high explosive close to a structural component results in a blast load that is highly localized and nonuniform in nature. Prediction of structural response and damage due to such loads requires a detailed understanding of both the magnitude and distribution of the load, which in turn are a function of the properties and dimensions of the structure, the standoff from the charge to the structure, and the composition of the explosive. It is common to express an explosive as an equivalent mass of TNT to facilitate the use of existing and well-established semi-empirical methods. This requires calculation of a TNT equivalency factor (EF), i.e. the mass ratio between the equivalent mass of TNT and the explosive mass in question, such that a chosen blast parameter will be the same for the same set of input conditions aside from explosive type. In this paper, we derive EF for three common explosives: C4, COMP-B, and ANFO, using an equivalent upper bound kinetic energy approach. A series of numerical simulations are performed, and the resultant magnitudes and distributions of specific impulse are used to derive the theoretical upper bound kinetic energy that would be imparted to a flexible target. Based on the equivalent mass of TNT of each explosive, which is required to impart the same kinetic energy for a given target size and standoff distance as of TNT, the EF is calculated. It is shown that in the near-field, the EFs are non-constant and are dependent on both standoff and target size. The results in the current study are presented in a scaled form and can be used for any practical combination of charge mass, distance from the charge to the target, target size, thickness, and density.

**Keywords:** TNT equivalency, Blast, Energy equivalent impulse, Near-field, Numerical analysis

---

<sup>1</sup> Corresponding author, e-mail: hezi@technion.ac.il

## 26 **1. Introduction**

27 The prediction of the blast wave parameters following detonation of a high explosive is important for the  
28 assessment of the dynamic response of a structure subjected to that load. The blast wave parameters, such as the  
29 peak overpressure and impulse, and the magnitude and distribution over the structural element significantly  
30 affect its dynamic response. Analytical methods for the prediction of the blast parameters are rarely available,  
31 and therefore, there are three main approaches for their evaluation, as follows:

- 32 I. Empirical (or semi-empirical) models, which are given in the form of equations or diagrams. Examples  
33 are the methods given in design manuals, such as the UFC 3-340-02 (USACE, 2008), or the commonly  
34 used equations given by (Kingery and Bulmash, 1984). Being such fast running tools, these models are  
35 preferred by engineers, although they are limited to geometrically simple scenarios and charge  
36 configurations.
- 37 II. Numerical simulations using hydro-codes (e.g. Grisaro and Edri, 2017; Shin et al., 2015). Although this  
38 approach is expensive in terms of computational time and resources, it provides more accurate results  
39 for complex geometries, various charge shapes, and close-in detonations.
- 40 III. Experimental studies for more specific and special cases (e.g. Codina and Ambrosini, 2018; Rigby et al.,  
41 2019a).

42 A structure that is exposed to a close-in detonation is expected to experience high magnitudes of overpressure  
43 and impulse. A close-in detonation is commonly defined for scaled distances that are lower than  $1.2 \text{ m/kg}^{1/3}$   
44 (ASCE, 2011; CSA, 2012; Ritchie et al., 2018). In addition to the high pressure and impulse magnitudes in the  
45 near-field regime, the blast load in such conditions is expected to be nonuniform over the loaded face of the  
46 structure. These aspects make the prediction of the blast load parameters nontrivial and challenging, especially  
47 by using simplified methods. Although such methods are very common due to their low computational cost,  
48 their accuracy in the near-field regime is doubtful. Furthermore, while empirical models consider an idealized  
49 spherical or hemispherical charge shapes, the charge shape may be different, and in the near-field regime, the  
50 shape may significantly affect the overpressure environment around the charge (Adhikary et al., 2017; Sherkar  
51 et al., 2014). Thus, the two other methods are frequently used. When experimental work is not possible or  
52 practical, i.e. when a large number of scenarios is of interest, numerical simulations may naturally be the  
53 preferable option.

54 Many of the above semi-empirical approaches assume the explosive is formed of TNT. However, when a  
55 different explosive is used, for the same charge mass, different blast parameters, such as the peak overpressure  
56 and impulse, are derived (Cooper, 1996; Esparza, 1986). In such cases, an equivalent charge mass of TNT is  
57 defined, which would yield the same blast load parameter (impulse, overpressure, etc.) at the same distance.  
58 The mass ratio of the equivalent TNT charge mass and the examined explosive mass is defined as the TNT  
59 equivalency factor (EF). Available methods (Grisaro and Edri, 2017) for predicting the EF values consider  
60 several parameters such as the internal charge energy, detonation velocity, Chapman-Jouguet pressure, and  
61 explosive density. In a previous study (Grisaro and Edri, 2017), it was found that for the far-field regime (for  
62  $3 \leq Z \leq 40 \text{ m/kg}^{1/3}$ ), both the EFs for impulse and overpressure strongly depend on the energy ratio of the examined

63 explosive and TNT. However, a different function of the energy ratio was found for the impulse and the peak  
64 overpressure. Also, it was found that a constant value of EF can be used for impulse and pressure for the entire  
65 range of scaled distances referring to the far-field regime. However, there are currently very few studies on TNT  
66 equivalency in the near-field regime. These studies show that unlike the far-field regime, in the near-field regime  
67 a unique EF value for a specific blast parameter cannot represent the real behavior (e.g. Xiao et al., 2020, 2019).  
68 Therefore, in addition to affecting the impulse and pressure values, the EF in the near-field may affect also the  
69 spatial distribution of the blast load over the structural element.

70 The response of thin plates subjected to close-in detonations was studied by (Rigby et al., 2019a), using a  
71 combination of experimental, numerical, and analytical tools. Since the blast load duration in a close-in  
72 detonation event is expected to be short compared to the period of vibration of the structure, the dominant load  
73 parameter is the impulse. The impulse distribution is expected to be nonuniform, as shown in Figure 1a. Thus,  
74 (Rigby et al., 2019a) defined an impulse enhancement factor, which enables a complex distributed load to be  
75 expressed as an equivalent uniform load which would impart the same kinetic energy to a target plate. It was  
76 shown that peak displacement was closely correlated to energy equivalent impulse, and weakly correlated to  
77 total impulse, therefore the peak displacement could be better predicted with knowledge of the distribution of  
78 loading, as well as its magnitude.

79 Assuming that a plate is subjected to nonuniform impulsive loading, the following cases are possible. Firstly,  
80 under the assumption that the deformation modes possess infinite resistance to shear as shown in Figure 1b, the  
81 entire plate acts as a rigid body and the deformation mode represents a lower bound of the kinetic energy. A  
82 second possible extreme scenario includes a deformation mode in which the shear resistance between two mass  
83 particles of the plate is zero. Therefore, in this case, the kinetic energy is characterized by its upper bound. It  
84 was also shown by (Rigby et al., 2019a) that two different targets, each experiencing a load that imparts the  
85 same upper bound kinetic energy, will experience similar dynamic peak displacement for different charge mass  
86 and scaled distance. Thus, the prediction of this parameter is essential for the comparison of the structural  
87 response between two different cases. In their study (Rigby et al., 2019a), a single type of explosive charge was  
88 studied (PE4).

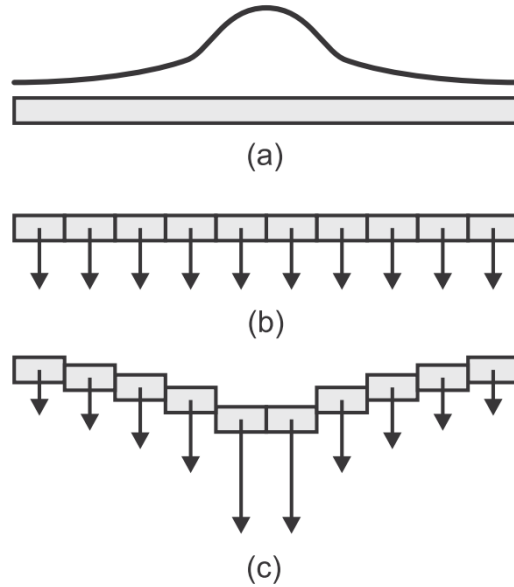


Figure 1 – Nonuniform impulse distribution (a), and modes of deformation related to lower bound (b) and upper bound (c) kinetic energy (Rigby et al., 2019a)

89 A motivation is raised from the previous information to study and assess the blast loading on plates in the near-  
 90 field regime, from different explosive types, but with the same mass and standoff distance. The specific impulse  
 91 distribution has the potential to be different for different explosive types, therefore the main goal of this study  
 92 is to define the EF for energy equivalent impulse, based on the scaled distance of the charge to the loaded plate  
 93 face, and the scaled plate dimensions. The main distinction between the current study and previous studies,  
 94 which dealt with TNT equivalency factors, is that in previous studies the EF was related to blast wave parameters  
 95 at a single point some distance from the explosive, while in the current study the EF is related to loading  
 96 distributions which are more closely related to dynamic structural response.

97 This paper focuses on the derivation and assessment of the TNT EF of three explosives: C4, COMP-B, and  
 98 ANFO. It is based on numerical hydro-code simulations and uses a common scaling theory. The EF is calculated  
 99 for each explosive and the results are presented in their scaled form. The paper is outlined as follows: The  
 100 methodology is explained in the following section, after which the numerical model is presented. The model is  
 101 validated and verified, and it is used for a parametric study for the assessment of the impulse magnitude and  
 102 distribution along the radius of a circular plate, for various scaled distances from the target and scaled target  
 103 sizes. Reference scaled data for TNT explosives is generated from the numerical simulation. The results for C4,  
 104 COMP-B, and ANFO are scaled and analyzed using the scaling laws to find the equivalent TNT charge which  
 105 yields the same upper bound kinetic energy that constitutes a representative measure of the dynamic structural  
 106 response.

## 107 **2. Methodology**

108 The case considered in the current study refers to the detonation of a spherical charge (initiated at its center)  
 109 close to a circular thin plate, as illustrated in Figure 2. The charge mass is  $W$ , the closest distance from the charge  
 110 center to the target is  $R$ , the target radius is  $a$ , and the coordinate along the target radius is  $0 \leq r \leq a$ . The coordinate

111  $r$  corresponds to an angle of  $\theta = \arctan(r/R)$  between the axisymmetric axis and a line connecting the charge  
 112 center and a point located at coordinate  $r$  along the radial direction of the target. The following definitions can  
 113 be made: The scaled distance between the charge center and the target is  $Z = R/W^{1/3}$ , and the scaled target radius  
 114 is  $z = a/W^{1/3}$ . Note that clearing effects are not considered in the current study.

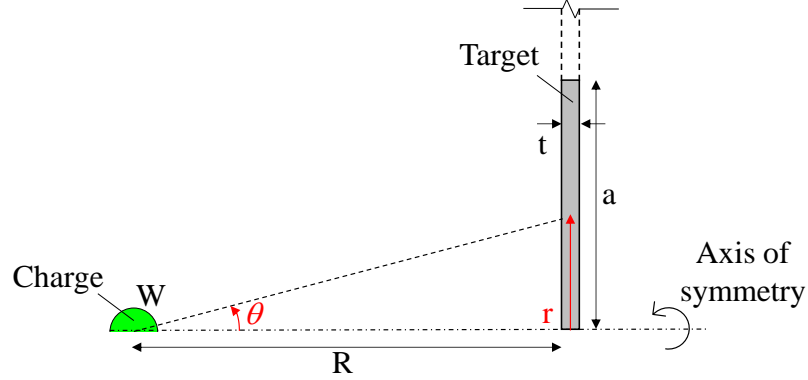


Figure 2 – Layout of the case considered in the current study (axisymmetric view)

115 As mentioned in the introduction section, the dominant parameter that should be compared between two loading  
 116 cases to get the same peak displacements is the upper bound kinetic energy of the structure  $E_{k,u}$  (Rigby et al.,  
 117 2019a) that reads:

$$E_{k,u} = \frac{1}{2\rho t} \int_A i^2(R, x, y) dA \quad (1)$$

118 where  $\rho$  is the density,  $t$  is the thickness,  $i$  is the nonuniform specific impulse (per unit area),  $A$  is the structure  
 119 surface area exposed to the blast load, and  $(x, y)$  are Cartesian coordinates on the target plate, where the origin  
 120 is the target center. Eq. (1) shows that the impulse distribution over the plate surface is a dominant parameter  
 121 affecting the kinetic energy. Note that overpressure does not appear in Eq. (1). Due to the high intensity and  
 122 short duration of the blast load compared to the period of vibrations of the structure, the loading condition is  
 123 considered impulsive, and the impulse is the only parameter that affects the structural response. In the current  
 124 study, the structure is a thin circular plate, and for that case, Eq. (1) can be rewritten in polar coordinates:

$$E_{k,u} = \frac{\pi}{\rho t} \int_{r=0}^{r=a} i^2(R, r) r dr \quad (2)$$

125 where  $i(R, r)$  is the impulse along the radial direction, measured from the circular plate center (see Figure 2).  
 126 The prediction of the blast load parameters follows the Hopkinson-Cranz scaling laws (Baker, 1973; Cooper,  
 127 1996), which are based on Buckingham  $\pi$  theorem. According to the scaling laws, the scaled impulse ( $i/W^{1/3}$ ) is  
 128 a function of the scaled distance  $Z$ . Since the main goal of the current study is to assess the upper bound kinetic  
 129 energy, it must be scaled as well. Therefore, we present a scaled form of the upper bound kinetic energy which

130 includes the scaled plate parameters (density, thickness, and radius) and the blast parameters (impulse and  
131 distance).

132 The EF for the structural response should be clearly defined. Since the upper bound kinetic energy depends on  
133 the scaled distance  $Z$  and the target size (defined by the angle of incidence  $\theta$ , or by the scaled plate radius  $z$ ),  
134 the definition of the equivalent TNT mass is as follows: The equivalent TNT mass is the mass of the examined  
135 explosive multiplied by EF, such that it would yield the same upper bound kinetic energy (and hence energy  
136 equivalent uniform impulsive load) for a TNT charge located at the same absolute distance from the plate, and  
137 for the same plate absolute dimensions.

138 The numerical model shown in Section 3 provides the impulse and its spatial distribution which is then used to  
139 calculate the upper bound kinetic energy. Thus, the numerical model has to be first validated with available  
140 experimental results. After its validation, the impulse distributions for various cases are used to calculate the  
141 upper bound kinetic energy in each case. The results for the upper bound kinetic energy for various plate sizes,  
142 standoff distances, and charge masses are first produced for TNT. Next, the data for TNT is taken as a reference  
143 data, to which the results of the other explosives are compared, to find their EF.

### 144 **3. Numerical modeling**

#### 145 **3.1 Geometry and materials**

146 The numerical models are solved in Ansys Autodyn hydro-code (Ansys, 2016). A typical numerical 2D  
147 axisymmetric model is shown in Figure 3, for 50 g TNT located 200 mm from the target. The model includes a  
148 400x400 mm<sup>2</sup> Eulerian mesh. The mesh is filled with air and spherical explosive charge (in the axisymmetric  
149 model, the spherical charge is represented by a semi-circle shape with its center located along the axisymmetric  
150 axis). The detonation point is assumed to be located at the charge center. The target is modeled as a rigid  
151 reflected boundary condition along the right vertical boundary, with the implicit assumption that no fluid-  
152 structure softening occurs (congruent with the impulsive nature of the loading). The other boundaries (excluding  
153 the axisymmetric axis) are modeled with “flow-out” boundary conditions, which allow the detonation products  
154 and pressures to vent from the model without any reflections. Numerical gauges are placed with intervals of 5  
155 mm along the target radius, to measure the reflected overpressure histories and thus determine specific impulse.

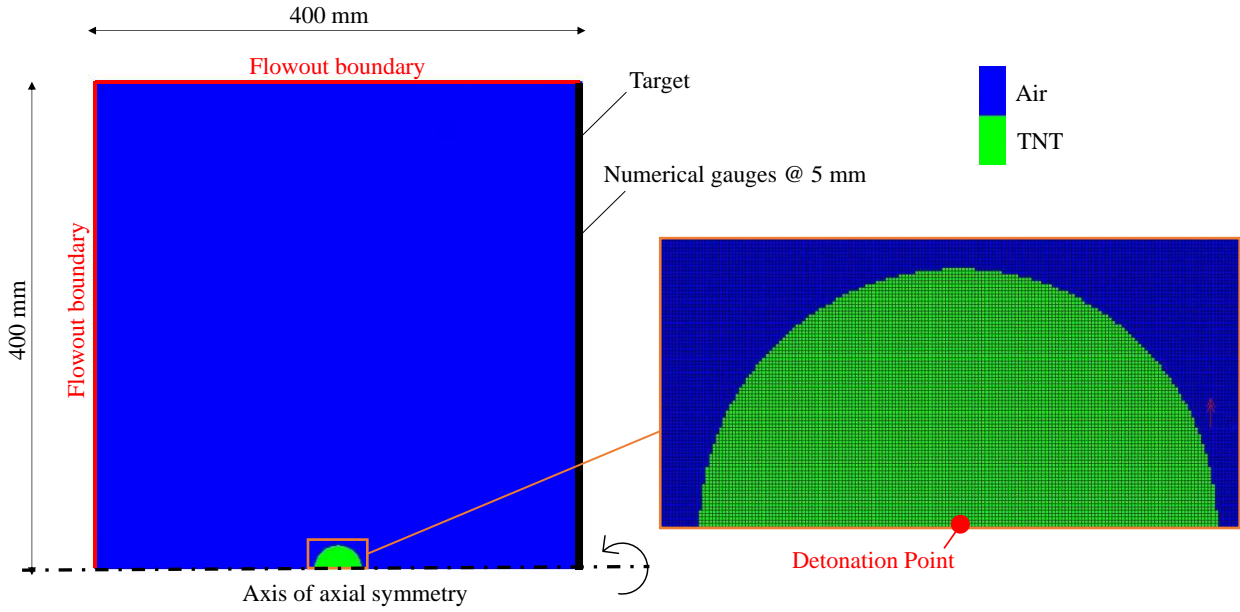


Figure 3 – Typical axisymmetric numerical model

156 The air is modeled with an ideal gas equation of state (EOS) as follows:

$$p = (\gamma - 1)\rho e \quad (3)$$

157 where  $p$  is the pressure,  $\gamma = 1.4$  is the heat capacity ratio,  $\rho$  is the density, and  $e$  is the internal energy per unit  
 158 mass. Initially, the air is assumed to be in standard conditions with a density of  $\rho = 1.225 \text{ kg/m}^3$  and a pressure  
 159 of  $p = 101.332 \text{ kPa}$ . The corresponding internal energy per unit mass is  $e = 0.206 \text{ MJ/kg}$ .

160 The explosives are modeled by the Jones-Wilkins-Lee (JWL) EOS (Ansys, 2016; Lee et al., 1968) as shown in  
 161 Eq. (4):

$$p = A_1 \left( 1 - \frac{w\rho}{R_1\rho_0} \right) e^{-R_1 \frac{\rho_0}{\rho}} + A_2 \left( 1 - \frac{w\rho}{R_2\rho_0} \right) e^{-R_2 \frac{\rho_0}{\rho}} + w\rho e \quad (4)$$

162 where  $\rho_0$  is a reference density.  $A_1$ ,  $A_2$ ,  $R_1$ ,  $R_2$ , and  $w$  are constants. The detonation velocity,  $D$ , and the Chapman-  
 163 Jouguet pressure,  $P_{CJ}$ , are also considered in Autodyn for the detonation process. Four types of explosives are  
 164 considered in the current study and their well-known JWL parameters are given in Table 1.



Table 1 – JWL EOS parameters for the examined explosives

| Explosive                   | $\rho_0$ (g/cm <sup>3</sup> ) | $A_1$ (kPa)        | $A_2$ (kPa)        | $R_1$ | $R_2$ | w    | e (MJ/kg) | D (m/s) | $P_{CJ}$ (GPa) |
|-----------------------------|-------------------------------|--------------------|--------------------|-------|-------|------|-----------|---------|----------------|
| TNT (Dobratz, 1985)         | 1.63                          | $3.712 \cdot 10^8$ | $3.231 \cdot 10^6$ | 4.15  | 0.95  | 0.30 | 4.294     | 6930    | 21.0           |
| ANFO (Davis and Hill, 2002) | 0.93                          | $4.946 \cdot 10^7$ | $1.891 \cdot 10^6$ | 3.91  | 1.12  | 0.33 | 2.668     | 4160    | 5.15           |
| C4 (Dobratz, 1985)          | 1.60                          | $6.098 \cdot 10^8$ | $1.295 \cdot 10^7$ | 4.50  | 1.40  | 0.25 | 5.621     | 8193    | 28             |
| COMP-B (Dobratz, 1985)      | 1.72                          | $5.242 \cdot 10^8$ | $7.678 \cdot 10^6$ | 4.20  | 1.10  | 0.34 | 4.950     | 7980    | 29.5           |

### 166 3.2 Convergence study and validation

167 Since a close-in detonation is modeled, the element size may be critical to achieving sufficient accuracy of the  
 168 results, and a mesh sensitivity analysis is therefore performed. The element size determined for a converged  
 169 solution is 0.25 mm, which corresponds to 2.56 million elements in the model. Figure 4 presents an example of  
 170 the difference between two simulations with two different meshes for 50 g TNT charge located at 50 mm from  
 171 the target. Results are presented for element sizes of 0.25 mm and 0.5 mm, which includes 640,000 elements.  
 172 Overall, there is a good agreement between the two cases, with some deviation concentrated in  $r \rightarrow 0$  and a  
 173 maximum difference of approximately 6% between the two cases. In view of the balance between accuracy and  
 174 computational effort, an element size of 0.25 mm was used to perform a parametric study. It should be noted  
 175 that for smaller mesh sizes the differences were negligible. A simulation with an element size of 0.25 mm  
 176 required about 12 hours run time in a standard Intel i7 desktop with 16 GB RAM.

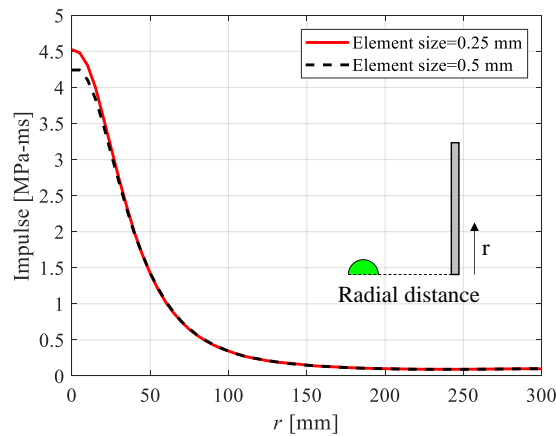


Figure 4 – Mesh sensitivity analysis for 50 g TNT located at 50 mm from the target

178 **3.3 Validation**

179 The numerical results are first validated by comparisons with experimental data. The experimental study of  
180 (Rigby et al., 2018, 2019a) in which 100 g spherical PE4 charges were detonated close to large, nominally rigid,  
181 circular target plates are used. In these tests, Hopkinson pressure bars were used to measure the reflected  
182 overpressure acting on the target along the radial direction. The present modeling uses the JWL parameters of  
183 C4 for the PE4 charge as the PE4 explosive is nominally identical to C4 (Rigby et al., 2019a). The impulse was  
184 calculated by numerically integrating the overpressure-time history measurements at each gauge with respect to  
185 time. Figure 5 shows the peak impulse along the radial direction (which is the vertical direction in the  
186 axisymmetric numerical model shown in Figure 3) and compares the numerical results with the experimental  
187 ones. The numerical results are within the scatter of the experimental data, and a good agreement is observed.

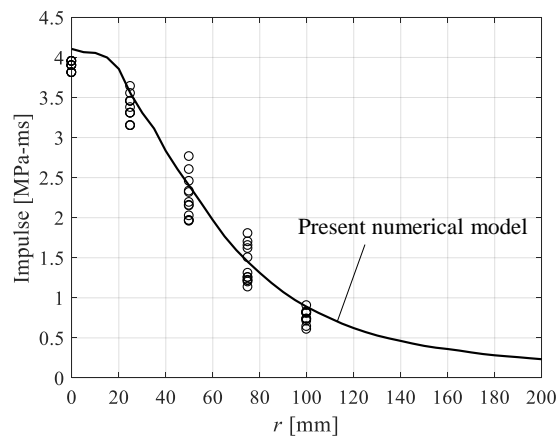


Figure 5 – Validation with experimental data from (Rigby et al., 2019b) for 100 g PE4 located 80 mm from the target

188 Further validation of the numerical model is achieved by comparing its results to the empirical diagrams given  
189 in UFC 3-340-02 (USACE, 2008) for TNT charges. In UFC 3-340-02, the scaled impulse is given as a function  
190 of the angle  $\theta$ . The comparison refers to two cases with scaled distances of  $Z = 0.198 \text{ m/kg}^{1/3}$  and  $Z = 0.784$   
191  $\text{m/kg}^{1/3}$ . The scaled impulse as a function of the angle of incidence for each case is presented in Figure 6. The  
192 numerical results are in good agreement with the TNT-standard empirical data provided in UFC 3-340-02.

193 The above findings demonstrate the validation and verification of the numerical model. The model is used in  
194 the next section for a parametric study to obtain the impulse distribution, which serves as an input parameter for  
195 calculating the target kinetic energy for various cases.

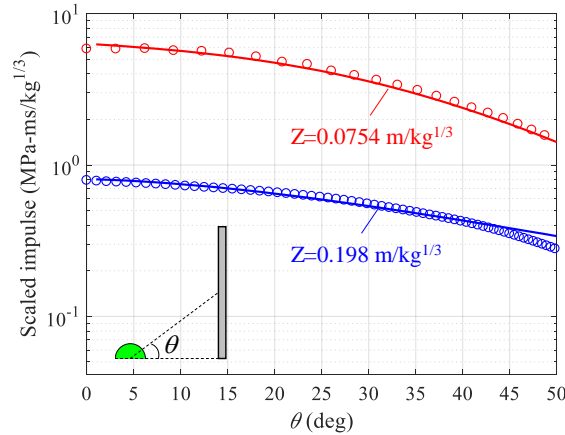


Figure 6 – Comparison with data from the UFC 3-340-02 (USACE, 2008) (solid line: UFC 3-340-02, circle markers: numerical model)

196 **4. Parametric study**

197 **4.1 Simulation plan**

198 The numerical model is used to perform a parametric study. Firstly, a set of numerical calculations are performed  
 199 to establish reference data for TNT, which is then used as the basis for the EF calculation of each explosive.  
 200 The simulation plan for TNT is shown in Table 2. The charge mass  $W$  varies from 0.308 to 50 g. The  
 201 distance  $R$  in Table 2 is defined as the distance between the charge center and the closest point on the target.  
 202 The corresponding scaled distance,  $Z = R/W^{1/3}$ , is calculated and shown in Table 2 as well, and they are in the  
 203 range  $0.136 < Z < 3.700 \text{ m/kg}^{1/3}$ . The distances  $R$  were chosen such that the absolute distance between the  
 204 charge center and the left vertical flow-out boundary will be no less than 150 mm to avoid any numerical effects  
 205 of this boundary on the reflected impulse distribution on the target.

Table 2 – Simulation plan for TNT

| $W$ (g) | $R$ (mm) | $Z$ ( $\text{m/kg}^{1/3}$ ) |
|---------|----------|-----------------------------|
| 50.000  | 50.0     | 0.136                       |
| 50.000  | 73.0     | 0.198                       |
| 50.000  | 100.0    | 0.271                       |
| 50.000  | 150.0    | 0.407                       |
| 50.000  | 200.0    | 0.543                       |
| 50.000  | 250.0    | 0.679                       |
| 2.000   | 150.0    | 1.191                       |
| 2.000   | 188.0    | 1.492                       |
| 2.000   | 220.0    | 1.746                       |
| 0.579   | 183.3    | 2.200                       |
| 0.579   | 216.7    | 2.600                       |
| 0.579   | 250.0    | 3.000                       |
| 0.416   | 250.0    | 3.350                       |
| 0.308   | 250.0    | 3.700                       |

206 After establishing the reference data for TNT, numerical simulations for ANFO, C4 and COMP-B have been  
 207 performed, and the simulation plan is shown in **Error! Reference source not found.** In total, 44 simulations  
 208 have been performed (14 simulations to achieve the reference data for TNT and 10 simulations for each  
 209 examined explosives). Note that the reference data for TNT is calculated up to  $Z = 3.7 \text{ m/kg}^{1/3}$ , while the data  
 210 for the examined explosives (ANFO, C4 and COMP-B) is calculated up to  $Z = 3 \text{ m/kg}^{1/3}$ . The reason is that the  
 211 value of the EF at  $Z = 3 \text{ m/kg}^{1/3}$  is expected to be calculated, and in the calculation of the EF, the intersection  
 212 point with the reference TNT curves may exist in the range of  $Z > 3 \text{ m/kg}^{1/3}$ .

Table 3 – Simulation plan for ANFO, C4 and COMP-B

| W (g)  | R (mm) | Z (m/kg <sup>1/3</sup> ) |
|--------|--------|--------------------------|
| 50.000 | 50     | 0.136                    |
| 50.000 | 73     | 0.198                    |
| 50.000 | 100    | 0.271                    |
| 50.000 | 150    | 0.407                    |
| 50.000 | 200    | 0.543                    |
| 50.000 | 250    | 0.679                    |
| 2.000  | 150    | 1.191                    |
| 2.000  | 188    | 1.492                    |
| 2.000  | 220    | 1.746                    |
| 0.579  | 250    | 3.000                    |

## 213 4.2 Upper bound kinetic energy calculation

214 As outlined previously, the results of the upper bound kinetic energy for TNT are taken as reference data for the  
 215 EF calculations. Because the impulse is given in discrete locations along the target radius, where the numerical  
 216 gauges were placed, the integral in Eq. (2) is numerically solved using the trapezoid numerical method. For each  
 217 numerical gauge,  $E_{k,u}$  is calculated, assuming that the gauge is located at the edge of a given circular plate (i.e.  
 218 the target radius  $a$  is equal to the radial position of the gauge). To describe more general results which can be  
 219 used in any parameter combination, a scaled form of Eq. (2) should be introduced. After scaling the impulse  $i$ ,  
 220 the target radius  $a$ , the coordinate along the target radius  $r$ , and the target thickness  $t$ , by  $W^{1/3}$ , the scaled form  
 221 of Eq. (2) is shown in Eq. (5). The density is not scaled according to the scaling theory.

$$\frac{E_{k,u}}{W} \rho \frac{t}{W^{1/3}} = \pi \int_{z=\frac{r}{W^{1/3}}=0}^{z=\frac{r}{W^{1/3}}=\frac{a}{W^{1/3}}} \frac{i^2}{W^{2/3}} \frac{r}{W^{1/3}} dz = f(Z, z) \quad (5)$$

222  $E_{k,u}$  depends on the determined values of the target thickness and density, as shown in Eq. (2). However, for the  
 223 implementation of the scaled form, any value for the thickness and density of the target can be randomly chosen  
 224 for the absolute value of  $E_{k,u}$  calculated by Eq. (2). Although the absolute value of  $E_{k,u}$  is divided by the target  
 225 density and the thickness (Eq. (2)), in the scaled form  $E_{k,u}$  is multiplied again by the same values (Eq. (5)), and

226 therefore, the same scaled value is achieved for any target thickness and density (the upper bound kinetic energy  
 227 relation is assumed to hold, provided the plates can still be considered thin and deform as a membrane). From  
 228 all simulations, the results are collected and for a given target defined by a scaled dimension  $z$ , or a constant  
 229 angle of incidence  $\theta$ , the upper bound kinetic energy is calculated as a function of the scaled distance  $Z$  between  
 230 the charge center and the target loaded face.

231 The upper bound kinetic energy was calculated and scaled for each explosive type from all simulations. Since  
 232  $E_{k,u}$  is a function of two variables, the left side of Eq. (5) is represented by a surface, defined by  $Z$  and  $z$ , for each  
 233 explosive. An example of the scaled surface for TNT is shown in Figure 7 in 2D contour form. Using the same  
 234 procedure, the surfaces were produced also for ANFO, C4, and COMP-B.

235 Figure 8 presents an example of a comparison between the scaled upper bound kinetic energy for a given scaled  
 236 target radius  $z = 0.4 \text{ m/kg}^{1/3}$ . Note that a gauge that is placed at a given radial distance is located at a different  
 237 scaled distance along the target radius if a different charge mass is used. Hence, in cases where there was no  
 238 gauge located at  $r = zW^{1/3}$  (where  $z = 0.4 \text{ m/kg}^{1/3}$  in this example), linear interpolation was applied to estimate  
 239 the value at  $z = 0.4 \text{ m/kg}^{1/3}$ . It can be seen that as the scaled distance  $Z$  increases, the energy decreases, as  
 240 expected. For the same conditions (same plate radius, thickness and density, and same standoff distance between  
 241 the charge and the plate), C4 yielded the highest value of the upper bound kinetic energy and ANFO yielded the  
 242 lowest one. Therefore, it is expected that there would be different EF values for each explosive, and there is a  
 243 motivation to study the variation of the EF with scaled distance and scaled target size.

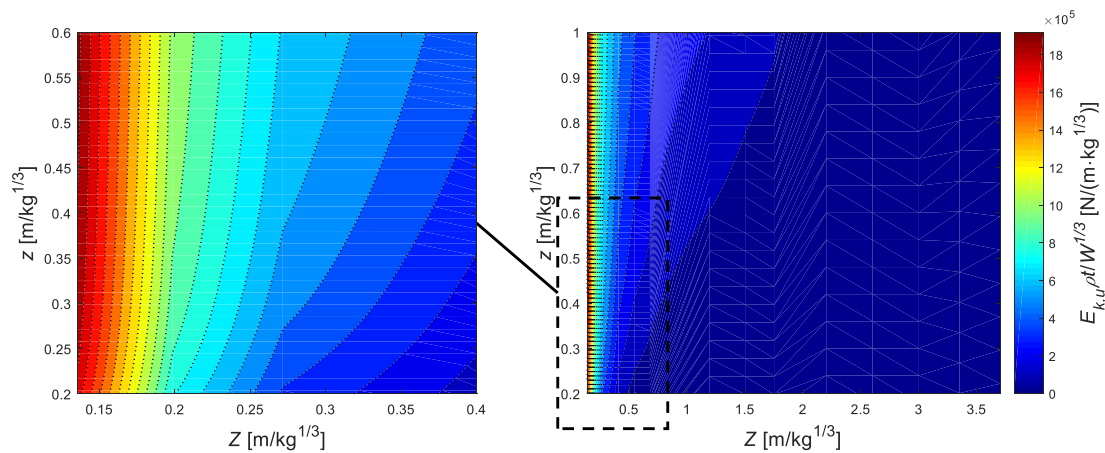


Figure 7 – Example of the scaled upper bound kinetic energy surface for TNT

244

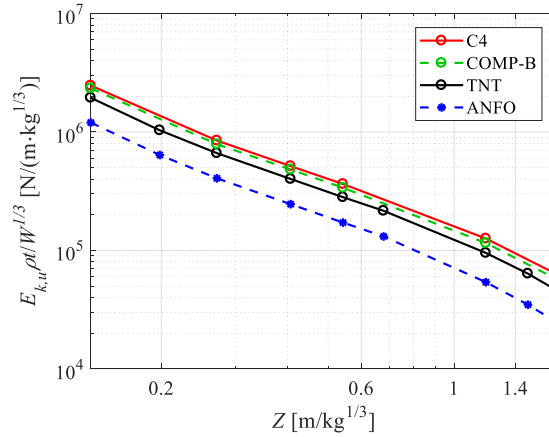


Figure 8 – Example of the scaled upper bound kinetic energy for different explosives and  $z = 0.4 \text{ m/kg}^{1/3}$

## 245 5. TNT equivalency factor (EF)

### 246 5.1 Calculation approach

247 The EF for the upper bound kinetic energy (and as a result, for structural response (Rigby et al., 2019a)) was  
 248 calculated based on blast scaling laws, as follows: It is evident that the upper bound kinetic energy for ANFO,  
 249 C4, and COMP-B is different than for TNT for the same conditions (same charge mass, absolute distance R,  
 250 target radius a, and target thickness). Therefore, in order to conserve upper bound kinetic energy (and hence  
 251 equivalent uniform impulse) when relating the examined explosive to an equivalent mass of TNT, the explosive  
 252 should be scaled to a different mass of TNT such that its scaled upper bound kinetic energy, scaled distance,  
 253 and scaled target size would lie on the TNT scaled curves. The results would be considered as the equivalent  
 254 TNT charge mass to use for the calculation of the EF. When the charge mass is changed, the scaled distance Z  
 255 and the scaled target radius z are also changed, because they depend on the charge mass. Thus, by changing a  
 256 point on the scaled surface of an explosive different to TNT by changing the charge mass, all three axes are  
 257 changed, where the main goal is to transfer this point to the scaled surface of TNT.

258 The solution is numerically achieved by using the following procedure: Assuming that the scaled surface of the  
 259 data for TNT is known:

$$\frac{E_{k,u}}{W} \cdot \rho \cdot \frac{t}{W^{1/3}} = f(Z, z) \quad (6)$$

260 where f is the surface function for TNT, the equivalent charge mass for the examined explosive is calculated for  
 261 a specific case by solving the following equation:

$$\frac{E_{k,u}}{W_{eq}} \cdot \rho \cdot \frac{t}{W_{eq}^{1/3}} = f\left(Z = \frac{R}{W_{eq}^{1/3}}, z = \frac{a}{W_{eq}^{1/3}}\right) \quad (7)$$

262 where  $E_{k,u}$  is the calculated upper bound kinetic energy for the examined explosive, located at a distance  $R$ , for  
 263 a target defined by the radius  $a$ .  
 264 The results for the EF are to be presented in scaled form for a given scaled target radius  $z$ . First, the scaled values  
 265 for a given  $z$  are found for the examined explosives, for each  $Z$  available from the numerical simulations. Eq.  
 266 (7) is solved using the bisection method. Throughout the numerical procedure, different values of  $W_{eq}$  are chosen  
 267 in an attempt to find the solution. By changing  $W_{eq}$ , the scaled target size  $z$  and the scaled distance  $Z$  are changed.  
 268 Since the function  $f$  of TNT must be used with the “new”  $z$  and  $Z$ , linear interpolation is applied to produce the  
 269 data between the known values derived from the numerical simulation. The solution provides the equivalent  
 270 charge mass  $W_{eq}$ , and the resulting EF is the ratio between the calculated equivalent charge mass  $W_{eq}$  and the  
 271 actual charge mass  $W$ , i.e.  $EF = W_{eq}/W$ .

272 **5.2 Results and discussion**

273 The EF is calculated for ANFO, C4, and COMP-B for scaled target sizes of  $z = 0.2, 0.4, \text{ and } 0.6 \text{ m/kg}^{1/3}$  by  
 274 applying the suggested procedure over a range of scaled distances. The variation of the EF with the scaled  
 275 distance  $Z$  for the three given values of  $z$  is shown in Figure 9, for the three examined explosives. Note that  
 276 linear interpolation was used in the numerical solution, which is an approximation of the variation between two  
 277 simulated points on the surface. The results are also presented in Table 4.

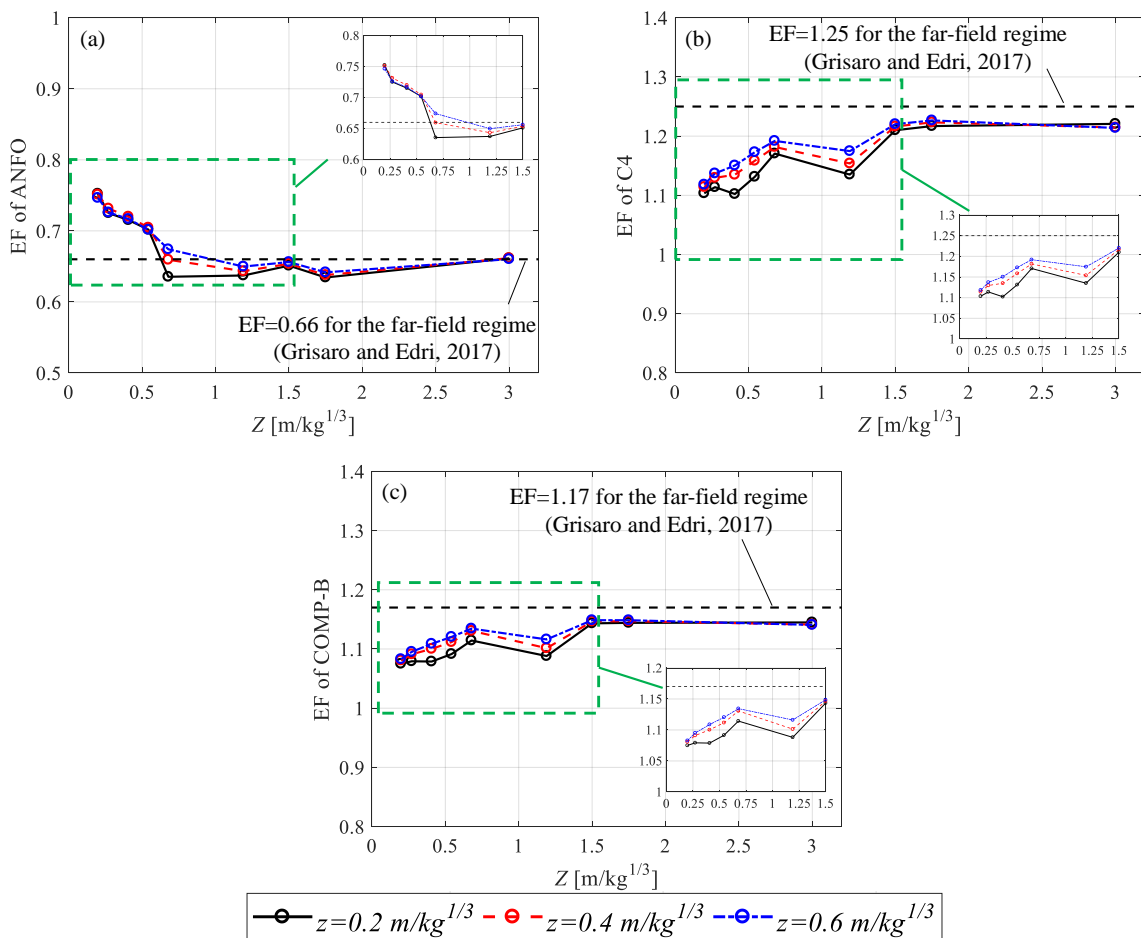


Figure 9 – Calculated EF values for (a) ANFO, (b) C4, and (c) COMP-B

Table 4 – Summary of the TNT equivalency results

| Z<br>(m/kg <sup>1/3</sup> ) | ANFO                           |                                |                                | C4                             |                                |                                | COMP-B                         |                                |                                |
|-----------------------------|--------------------------------|--------------------------------|--------------------------------|--------------------------------|--------------------------------|--------------------------------|--------------------------------|--------------------------------|--------------------------------|
|                             | z = 0.2<br>m/kg <sup>1/3</sup> | z = 0.4<br>m/kg <sup>1/3</sup> | z = 0.6<br>m/kg <sup>1/3</sup> | z = 0.2<br>m/kg <sup>1/3</sup> | z = 0.4<br>m/kg <sup>1/3</sup> | z = 0.6<br>m/kg <sup>1/3</sup> | z = 0.2<br>m/kg <sup>1/3</sup> | z = 0.4<br>m/kg <sup>1/3</sup> | z = 0.6<br>m/kg <sup>1/3</sup> |
| 0.198                       | 0.75                           | 0.75                           | 0.75                           | 1.10                           | 1.11                           | 1.12                           | 1.08                           | 1.08                           | 1.08                           |
| 0.271                       | 0.73                           | 0.73                           | 0.73                           | 1.11                           | 1.13                           | 1.14                           | 1.08                           | 1.09                           | 1.10                           |
| 0.407                       | 0.72                           | 0.72                           | 0.72                           | 1.10                           | 1.13                           | 1.15                           | 1.08                           | 1.10                           | 1.11                           |
| 0.543                       | 0.70                           | 0.70                           | 0.70                           | 1.13                           | 1.16                           | 1.17                           | 1.09                           | 1.11                           | 1.12                           |
| 0.679                       | 0.64                           | 0.66                           | 0.67                           | 1.17                           | 1.18                           | 1.19                           | 1.11                           | 1.13                           | 1.13                           |
| 1.191                       | 0.64                           | 0.64                           | 0.65                           | 1.14                           | 1.15                           | 1.17                           | 1.09                           | 1.10                           | 1.12                           |
| 1.492                       | 0.65                           | 0.65                           | 0.66                           | 1.21                           | 1.22                           | 1.22                           | 1.14                           | 1.15                           | 1.15                           |
| 1.746                       | 0.63                           | 0.64                           | 0.64                           | 1.22                           | 1.22                           | 1.23                           | 1.14                           | 1.15                           | 1.15                           |
| 3.000                       | 0.66                           | 0.66                           | 0.66                           | 1.22                           | 1.21                           | 1.21                           | 1.14                           | 1.14                           | 1.14                           |

279

280 Opposed to the EF values derived in previous studies for the far-field (e.g. Grisaro and Edri, 2017), the  
 281 calculated EF values for the three examined explosives vary with the scaled distance Z, for a given scaled target  
 282 size z. However, the variations are quite moderate with the scaled distance. The EFs for C4 and COMP-B are  
 283 larger than 1.0, and the EF for ANFO is smaller than 1.0, as expected.

284 The EFs of ANFO, C4, and COMP-B for far-field explosions were found to be ~0.66, ~1.25, and ~1.17,  
 285 respectively (Grisaro and Edri, 2017). An interesting observation in this study shows that the EF values for these  
 286 three explosives converge to these values, as the scaled distance increases (see Figure 9 and Table 4). ANFO  
 287 converges more closely to the far-field EF values, whereas C4 and COMP-B converge to a value slightly below  
 288 the (Grisaro and Edri, 2017) values. Within this observation, the EFs of C4 and COMP-B increases as the scaled  
 289 distance Z increases, while it was found that the EF for ANFO decreases as Z increases. Our values for the EF  
 290 for ANFO, C4 and COMP-B in the far-field regime are 0.0%, -2.5% and -2.4% lower than the values obtained  
 291 by (Grisaro and Edri, 2017), respectively.

292 By changing the scaled target size z, there is a variation between the calculated EF values for C4 and COMP-B,  
 293 while for ANFO the differences are smaller. In all cases, for the larger Z, which is closer to the far-field regime,  
 294 the differences are negligible. Since specific impulse distribution is affected by explosive type, and different EF  
 295 values are derived for different scaled distances Z, for the largest examined value of Z the impulse distribution  
 296 is more uniform and the effect of target size is therefore less significant. Hence the EF values for increasing Z  
 297 approach those calculated for far-field conditions in a previous study (Grisaro and Edri, 2017), and the effect of  
 298 the nonuniform distribution is less significant.



## 299 **6. Summary and conclusions**

300 While TNT equivalency has been previously studied in terms of the blast wave parameters, in the current study,  
301 it is studied in terms of the structural response of thin plates under close-in detonations. Accordingly, the  
302 equivalency factors are calculated with respect to the upper bound kinetic energy, which was demonstrated to  
303 represent a physical measure for the resultant peak dynamic displacement of the plate (Rigby et al., 2019a). The  
304 study is based on numerical simulations, which are validated against experimental results and simplified  
305 methods. A parametric study is presented, which includes four types of explosives (TNT, ANFO, COMP-B,  
306 and C4) placed at various distances from a circular target with various radii. The impulse distribution along the  
307 target radial direction, and as a result, the upper bound kinetic energy, are calculated for each simulation and  
308 each target size. The TNT equivalency factors are calculated based on analytical considerations and blast wave  
309 scaling laws.

310 The following conclusions are drawn from the current study:

- 311 • Unlike the behavior observed in far-field loading conditions, the TNT equivalency factors have been  
312 found to vary with the scaled distance in the near-field regime. For the largest scaled distance examined  
313 in this study, the EFs tend to converge on the values that have been found in previous studies dealing  
314 with far-field explosions. In addition, a change in the scaled target size,  $z$ , has a decreasing effect on the  
315 variation of the TNT equivalency factors with increasing scaled distance  $Z$ .
- 316 • For C4 and COMP-B, an increase of the equivalency factors has been observed when increasing the  
317 scaled distance  $Z$ . However, for ANFO, the opposite trend has been found, and smaller TNT  
318 equivalency factors have been obtained for increasing scaled distances.
- 319 • The results in the current study have been presented in a scaled form and therefore they can be used for  
320 any combination of charge mass, distance from the charge to the target, target size, thickness, and  
321 density. As far as the scaled parameters are within the examined scaled limits, no further analyses are  
322 required to predict the EF given by the nonuniform impulse distribution acting on the target face.
- 323 • The approach presented in the current study includes the following limitations: the analyzed target is  
324 relatively thin, and the energy is calculated based on the assumption that there is no variation of the  
325 velocity and mass across the target thickness. The clearing effect is ignored. The material constitutive  
326 law of the target is linear and any nonlinear effects, accumulation of damage, and potential failure  
327 mechanism throughout the response are ignored.
- 328 • The results presented in the current paper refer to a spherical charge shape. It is known that charge shape  
329 has a significant effect on the blast parameters in the near-field, and therefore, on the structural response,  
330 so additional EFs would need to be calculated if the explosive was formed into a different shape. In  
331 addition, the charges are detonated at their centroid (i.e. at the center of the sphere) and the point of  
332 detonation may affect the impulse distribution in the near-field. However, these features can be easily  
333 addressed, and the proposed approach can be augmented to consider their effects on the results.

- 334 • The approach presented in the current paper is novel, and it provides important insight regarding the  
335 TNT equivalency in the near-field which may be used as a first step when analyzing the blast response  
336 of structures under close-in detonations.

## 337 **References**

- 338 Adhikary, S. Das, Chandra, L.R., Christian, A., Ong, K.C.G., 2017. Influence of cylindrical charge orientation  
339 on the blast response of high strength concrete panels. *Eng. Struct.* 149, 35–49.  
340 <https://doi.org/10.1016/J.ENGSTRUCT.2016.04.035>
- 341 Ansys, 2016. Ansys Autodyn 17.0, Theory manual.
- 342 ASCE, 2011. Blast protection of buildings, ASCE/SEI 59-11, American Society of Civil Engineers. Reston,  
343 VA.
- 344 Baker, W.E., 1973. Explosions in air. University of Texas Press.
- 345 Codina, R., Ambrosini, D., 2018. Full-scale testing of leakage of blast waves inside a partially vented room  
346 exposed to external air blast loading. *Shock Waves* 28, 227–241. [https://doi.org/10.1007/s00193-017-](https://doi.org/10.1007/s00193-017-0733-9)  
347 [0733-9](https://doi.org/10.1007/s00193-017-0733-9)
- 348 Cooper, P.W., 1996. Explosives engineering. Wiley-VCH.
- 349 CSA, 2012. Design and assessment of buildings subjected to blast loads, CSA S850-12, Canadian Standards  
350 Association. Mississauga, Ontario, Canada.
- 351 Davis, L.L., Hill, L.G., 2002. ANFO Cylinder Tests, in: Shock Compression of Condensed Matter - 2001: 12th  
352 Aps Topical Conference. AIP, Atlanta, Georgia, USA. <https://doi.org/10.1063/1.1483507>
- 353 Dobratz, B., 1985. LLNL explosives handbook : properties of chemical explosives and explosive simulants.  
354 Lawrence Livermore National Laboratory, Livermore, CA.
- 355 Esparza, E.D., 1986. Blast measurements and equivalency for spherical charges at small scaled distances. *Int.*  
356 *J. Impact Eng.* 4, 23–40. [https://doi.org/10.1016/0734-743X\(86\)90025-4](https://doi.org/10.1016/0734-743X(86)90025-4)
- 357 Grisaro, H.Y., Edri, I.E., 2017. Numerical investigation of explosive bare charge equivalent weight. *Int. J. Prot.*  
358 *Struct.* 8, 199–220. <https://doi.org/10.1177/2041419617700256>
- 359 Kingery, C.N., Bulmash, G., 1984. Air blast parameters from TNT spherical air burst and hemispherical surface  
360 burst. US Army Ballistic Research Laboratory technical report ARBRL-TR 02555. Maryland, USA.
- 361 Lee, E.L., Hornig, H.C., Kury, J.W., 1968. Adiabatic expansion of high explosive detonation products. Report  
362 UCRL-50422. University of California, Livermore, CA, USA.
- 363 Rigby, S., Fuller, B., Tyas, A., 2018. Validation of near-field blast loading in LS-Dyna, in: 5th International  
364 Conference on Protective Structures (ICPS5). Poznan, Poland, Poland.
- 365 Rigby, S., Akintaro, O., Fuller, B., Tyas, A., Curry, R., Langdon, G., Pope, D., 2019a. Predicting the response  
366 of plates subjected to near-field explosions using an energy equivalent impulse. *Int. J. Impact Eng.* 128,  
367 24–36. <https://doi.org/10.1016/J.IJIMPENG.2019.01.014>
- 368 Rigby, S., Tyas, A., Curry, R., Langdon, G., 2019b. Experimental Measurement of Specific Impulse Distribution  
369 and Transient Deformation of Plates Subjected to Near-Field Explosive Blasts. *Exp. Mech.* 59, 163–178.

370 <https://doi.org/10.1007/s11340-018-00438-3>

371 Ritchie, C.B., Packer, J.A., Seica, M. V., Zhao, X.-L., 2018. Behaviour and analysis of concrete-filled  
372 rectangular hollow sections subject to blast loading. *J. Constr. Steel Res.* 147, 340–359.  
373 <https://doi.org/10.1016/J.JCSR.2018.04.027>

374 Sherkar, P., Whittaker, A., Aref, A., 2014. On the Influence of Charge Shape, Orientation and Point of  
375 Detonation on Air-Blast Loadings, in: *Structures Congress 2014*. American Society of Civil Engineers,  
376 Reston, VA, pp. 68–73. <https://doi.org/10.1061/9780784413357.007>

377 Shin, J., Whittaker, A., Cormie, D., 2015. Estimating incident and reflected air - blast parameters : updated  
378 design charts, in: *16th International Symposium for the Interaction of the Effects of Munitions with*  
379 *Structures (ISIEMS 16)*. Destin, FL, USA.

380 USACE, 2008. Unified Facilities Criteria (UFC) - Structures to resist the effects of accidental explosions. UFC  
381 3-340-02, U.S Army Corps of Engineers.

382 Xiao, W., Andrae, M., Gebbeken, N., 2020. Air Blast TNT Equivalence Concept for Blast-Resistant Design.  
383 *Int. J. Mech. Sci.* 105871. <https://doi.org/10.1016/j.ijmecsci.2020.105871>

384 Xiao, W., Andrae, M., Gebbeken, N., 2019. Air blast TNT equivalence factors of high explosive material PETN  
385 for bare charges. *J. Hazard. Mater.* 377, 152–162. <https://doi.org/10.1016/j.jhazmat.2019.05.078>

386